Complex structures of different $CaFe_2As_2$ samples

B. Saparov*[,1], C. Cantoni[1], M. Pan[1], T. C. Hogan[2], W. Ratcliff II[3], S. D. Wilson[2], K. Fritsch[4], B. D. Gaulin[4,5,6] & A. S. Sefat[1]

[1]Oak Ridge National Laboratory, Oak Ridge, TN 37831, USA

[2]Department of Physics, Boston College, Chestnut Hill, MA 02467, USA

[3]NIST Center for Neutron Research, Gaithersburg, MD 20899-6102, USA

[4]Department of Physics and Astronomy, McMaster University, Hamilton, Ontario L8S 4M1, Canada

[5]Brockhouse Institute for Materials Research, McMaster University, Hamilton, Ontario L8S 4M1, Canada

[6]Canadian Institute for Advanced Research, 180 Dundas St W, Toronto, Ontario M5G 1Z8, Canada

*Correspondence to saparovbi@ornl.gov

Supporting Information

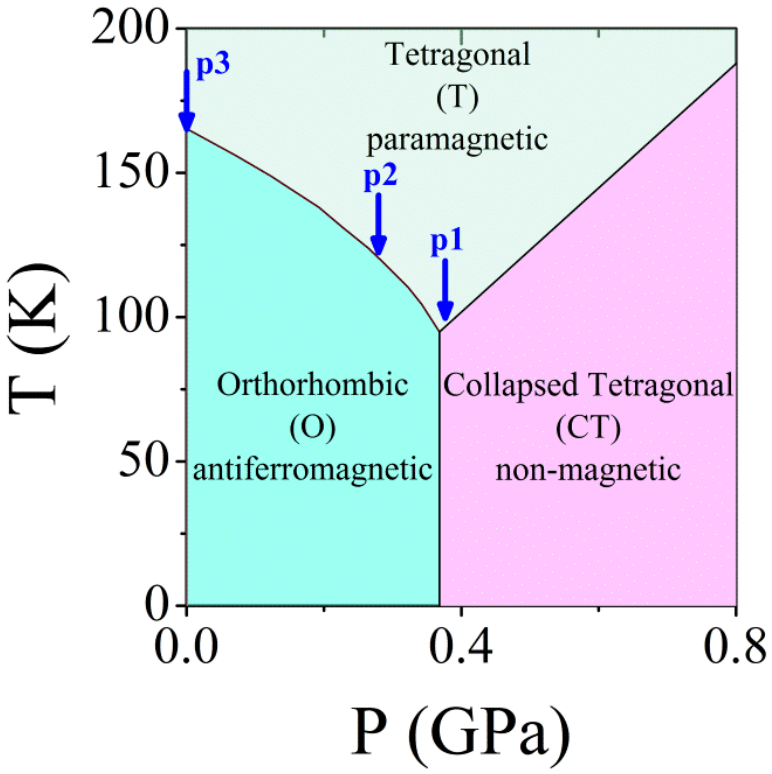

Figure S1. Temperature (T) – pressure (P) phase diagram of $CaFe_2As_2$; the data are adapted from references [10, 19, S1-S2]. Different parts of this phase diagram are reached here by annealing of the crystals [7]. The three samples studied in this manuscript are indicated as p1, p2 and p3. P1 undergoes a transition from paramagnetic tetragonal phase (T) to nonmagnetic collapsed tetragonal phase (CT) below 95(1) K, p2 and p3 samples transition from tetragonal to antiferromagnetic orthorhombic phases (O) at 168(1) K and 118(4) K, respectively.

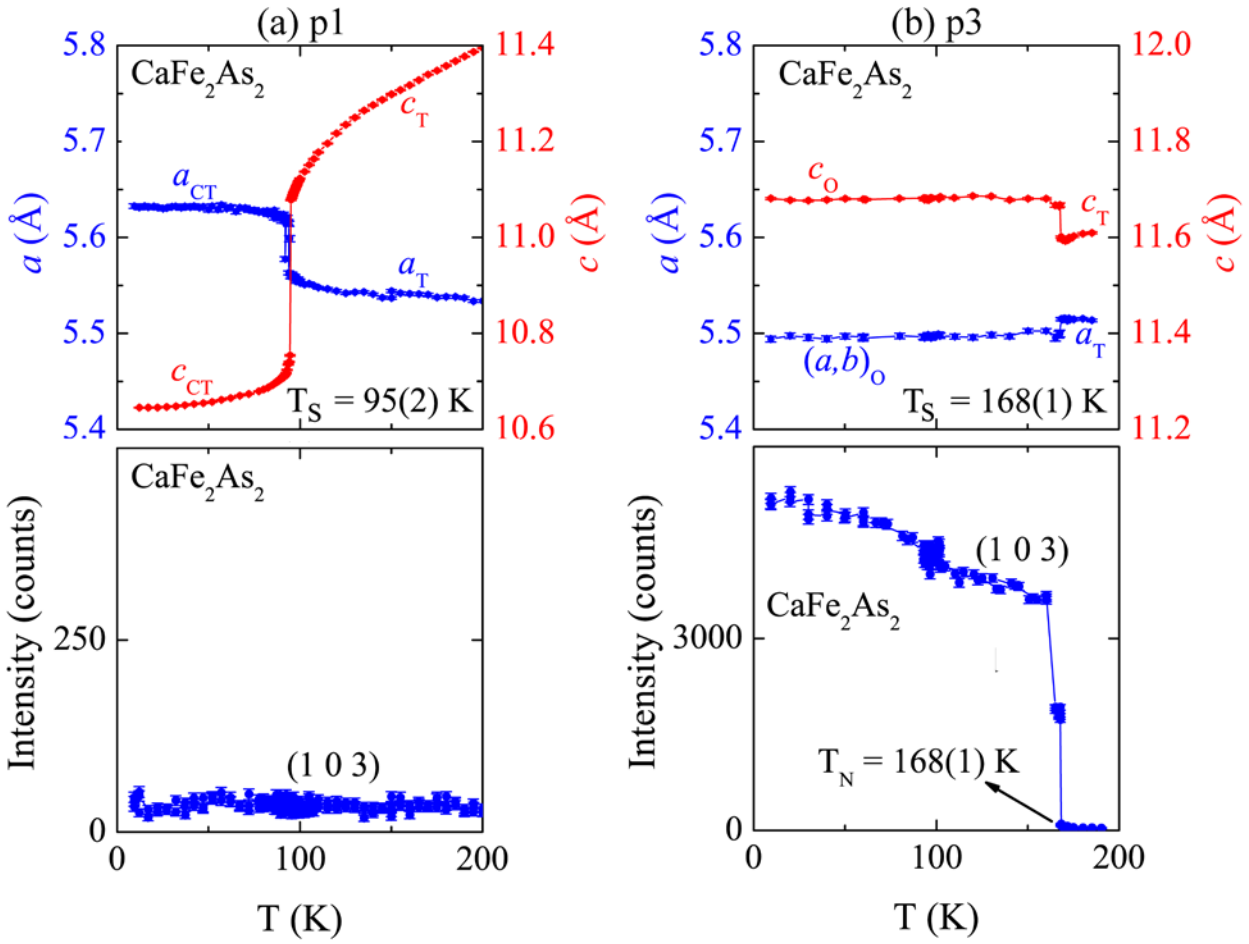

Figure S2. For $CaFe_2As_2$, temperature dependence of lattice parameters and intensity of (1 0 3) magnetic peaks obtained from neutron diffraction. (a) P1 transitions from a paramagnetic tetragonal (T) to a nonmagnetic collapsed tetragonal phase (CT) at T_S = 95(2) K, whereas (b) p3 undergoes a structural transition into an antiferromagnetic orthorhombic phase (O) at $T_S = T_N$ = 168(1) K. Error bars represent +/- one standard deviation. Tetragonal *a*-lattice parameters are multiplied by √2 for comparison.

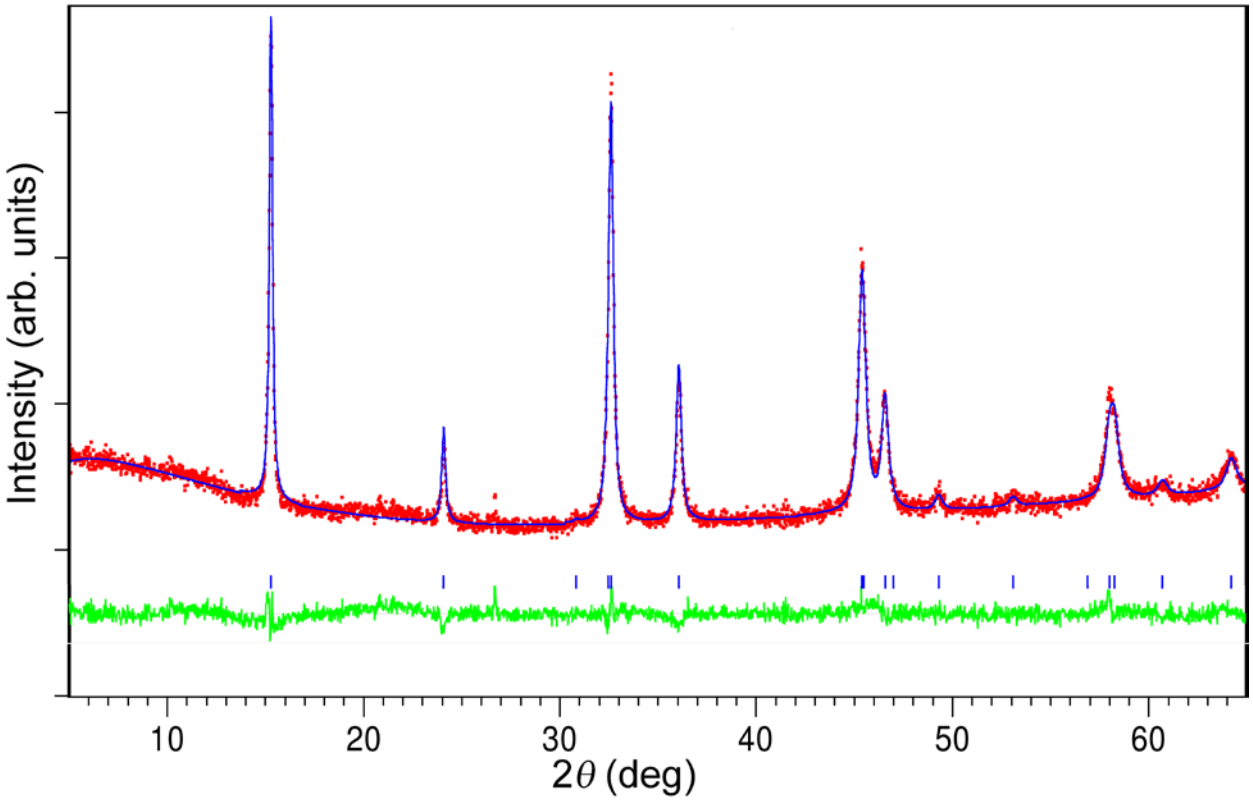

Figure S3. Rietveld refinement (blue line) of powder X-ray diffraction data (red dots) for as-grown p1 sample of $CaFe_2As_2$. The Bragg positions and difference plot are shown as blue tick marks and a green line, respectively.

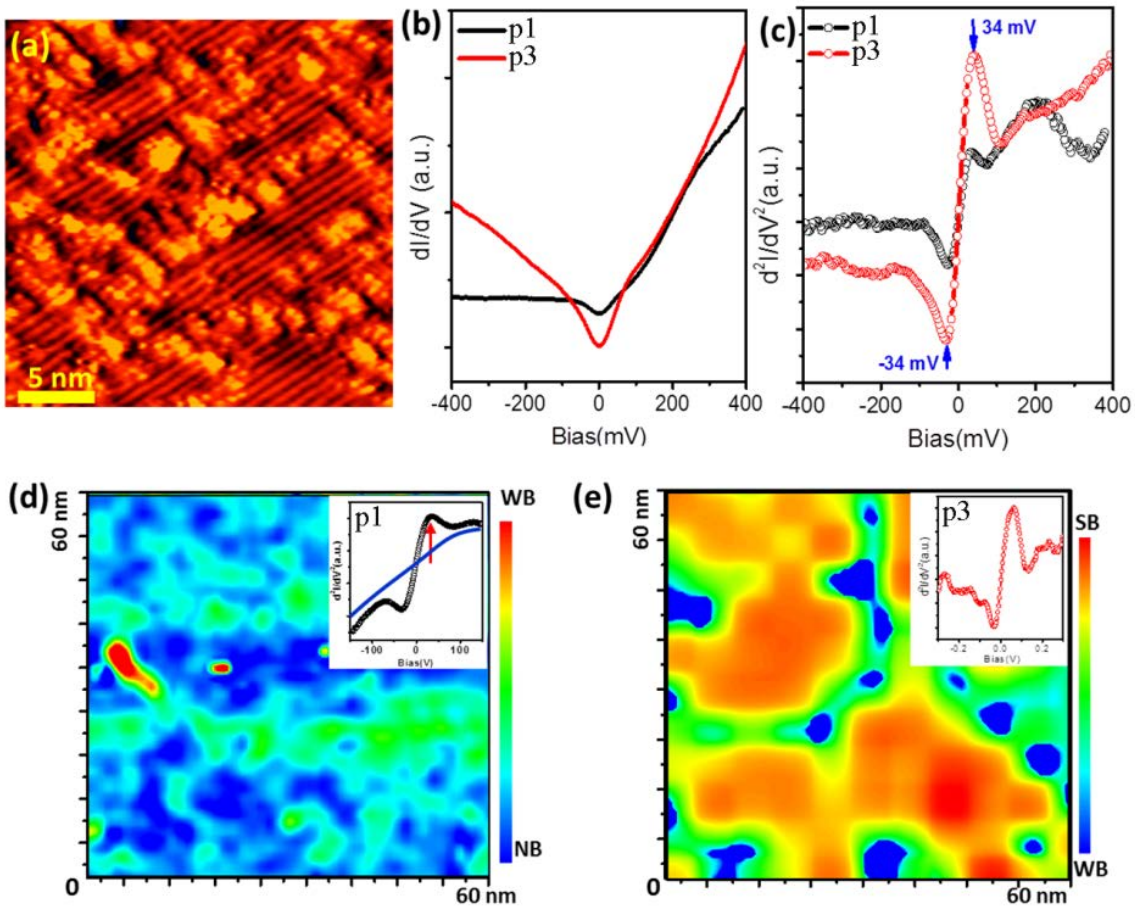

Figure S4. For $CaFe_2As_2$, (a) 24 nm × 24 nm STM topographic image for a cleaved p3 surface, taken with bias = 0.8 V, I_t = 20 pA, shows "2×1" stripes. (b) Averaged dI/dV spectra observed on the surface of p1 (black curve) and p3 (red curve), showing a V-shape with small kinks located symmetrically at both positive and negative biases. Such spectra are averaged from 50 × 50 dI/dV spectra grid over a larger area of 200 nm × 200 nm size on both $CaFe_2As_2$ samples, in order to eliminate the effect from spatial inhomogeneity in the area. (c) The second derivative d^2I/dV^2 versus V curve, derived numerically from dI/dV spectra in the panel (b). The bosonic mode appears at 34 mV as a pair of peak and dip. Spatial mapping of bosonic mode in (d) p1 and (e) p3 samples; a slice-cut with a fixed bias at +34 mV taken from experimental d^2I/dV^2 spectra grid measurement over a larger area of 60 nm × 60 nm size. Insets of (d) and (e) show representative d^2I/dV^2 spectra for strong (SB, red), weak (WB, black), and no (NB, blue) bosonic mode regions. The spectra were taken at 78 K with bias = -100mV, tunneling current = 100pA, and modulation V =35 mV.

Scanning Tunneling Microscopy (STM) and Scanning Tunneling Spectroscopy (STS): Figure S4a shows a topographic scanning tunneling microscopy (STM) image for the in situ-cleaved $CaFe_2As_2$ p3 crystal. In this image (24 nm × 24 nm), the majority of the sample surface is covered by so-called "2×1" stripes. As the in-plane lattice constant is 3.98 Å (consistent with low temperature neutron diffraction data), a high resolution image of stripes, reveals a 2×1 (8 Å × 4 Å) structure. Such 2×1 stripe structure has been frequently reported on the surface of various 122 Fe-based superconductors[S3-5], resulting from a half layer of alkaline-earth metal, after cleaving. Beside the stripes, the surface is also interrupted by some clusters, which are most likely remnants from room-temperature cleaving. To investigate the electronic difference between p1 and p3 samples, we measured the tunneling spectra at 78 K, which is well below T_N = 168(1) K in p3 sample. Because point tunneling spectra by STM is a very local measurement, in order to eliminate the effect of spatial inhomogeneity, we took the differential tunneling conductance spectra (dI/dV versus V) survey on a large surface area (200 nm × 200 nm). Figure S4b shows two dI/dV spectra, for each crystal averaged over 2500 curves. Such spatial averaged spectra can represent the electronic property of the materials. Both curves exhibit a similar, asymmetric overall V-shape background. The scanning tunneling spectroscopy (STS) on p3 demonstrates prominent "kinks" located symmetrically at both positive and negative biases. The peak-dip-hump feature has been observed in STS in both cuprates[S6,S7] and FeSCs[S8,S9]. A dip-hump feature appearing at certain voltage, resulted from inelastic tunneling and is believed to reveal a bosonic excitation, probably indicating spin-fluctuation mediated superconductivity in these materials. However, it is still debated whether such bosonic mode is induced by the interaction between the electrons and a phonon mode or associated with spin excitations. Such bosonic excitation can be observed clearly in the second derivative of the tunneling spectrum, that is, d^2I/dV^2 versus V. Clear dips (or peaks) should be observed in d^2I/dV^2 curve at energies of the bosonic excitation. By taking numerical derivative from the dI/dV spectra in Figure S4b, the corresponding d^2I/dV^2 curves are shown in Figure S4c. Sample P3 exhibits a pair of dip/peak at the energy of ±34 meV due to strong bosonic excitations[S10] or flat optical phonon modes located at 32-34 meV[S11]. We cannot unequivocally rule out either one of these scenarios, and choose to focus on the former scenario; in this case, the peaks at ±34 meV in d^2I/dV^2 curve represent the integration over spin wave excitations observed in $CaFe_2As_2$[S10], which explain the broadening of inelastic spectrum. In comparison, the d^2I/dV^2 spectrum (black curve) on sample p1 shows a much weaker dip (or peak) feature. Contrasting the antiferromagnetic p3 and nonmagnetic p1, the different intensities of dips (or peaks) in d^2I/dV^2 spectra strongly imply the observed bosonic excitation is originated from spin excitations in antiferromagnetic ordering of this material, instead of phonons. Such bosonic excitation is not necessarily relevant for superconductivity, as they can be observed in the non-superconducting $CaFe_2As_2$ parent. Instead of taking the numerical derivative of the dI/dV spectra, we measured d^2I/dV^2 spectrum experimentally by detecting the secondary harmonic of tunneling current with a lock-in technique. In Figure S4d and S4e, the colored maps illustrate the spatial distribution of such bosonic excitation in p1 and p3 surfaces, where the value of d^2I/dV^2 is represented in a color scale as a function of spatial

position with a fixed bias at +34 meV. It is evident that some areas show weak bosonic excitation, while other regions exhibit no-bosonic excitation. The corresponding d^2I/dV^2 curves are shown in the insets of Figure S4d and S4e, where the black curve shows a weak bosonic dip (or peak) and the blue curve has no bosonic feature. Therefore, we can conclude that there is a strong inhomogeneity of bosonic excitations in p1, which suggests a weak or non-antiferromagnetic ordering. These findings are consistent with our X-ray and neutron diffraction results in that there is a strongly inhomogeneous strain distribution in p1 with the minority of domains remaining in the uncollapsed magnetic state at low temperatures, while the majority of crystalline domains transition into the collapsed nonmagnetic state.

References

S1. Torikachvili, M. S., Bud'ko, S. L., Ni, N. & Canfield, P. C. Pressure induced superconductivity in $CaFe_2As_2$. *Phys. Rev. Lett.* **101**, 057006 (2008).

S2. Goldman, A. I. *et al.* Lattice collapse and quenching of magnetism in $CaFe_2As_2$ under pressure: a single crystal neutron and x-ray diffraction investigation. *Phys. Rev. B* **79**, 024513 (2009).

S3. Yin, Y., Zech, M., Williams, T. L., Wang, X., Wu, G., Chen, X. H. & Hoffman, J. E. Scanning tunneling spectroscopy and vortex imaging in the iron pnictide superconductor $BaFe_{1.8}Co_{0.2}As_2$. *Phys. Rev. Lett.* **102**, 097002 (2009).

S4. Zhang, H. *et al.* $\sqrt{2} \times \sqrt{2}$ structure and charge inhomogeneity at the surface of superconducting $BaFe_{2-x}Co_xAs_2$ ($x = 0 - 0.32$). *Phys. Rev. B* **81**, 104520 (2010).

S5. Massee, F., de Jong, S., Huang, Y., Kaas, J., van Heumen, E., Goedkoop, J. & Golden, M. Cleavage surfaces of the $BaFe_{2-x}Co_xAs_2$ and $Fe_ySe_{1-x}Te_x$ superconductors: a combined STM plus LEED study. *Phys. Rev. B* **80**, 140507 (2009).

S6. Lee, J. *et al.* Interplay of electron-lattice interactions and superconductivity in $Bi_2Sr_2CaCu_2O_{8+\delta}$. *Nature* **442**, 546-550 (2006).

S7. Niestemski, F. C., Kunwar, S., Zhou, S., Li, S., Ding, H., Wang, Z., Dai, P. & Madhavan, V. A distinct bosonic mode in an electron-doped high-transition-temperature superconductor. *Nature* **450**, 1058-1061 (2007).

S8. Shan, L. *et al.* Evidence of a spin resonance mode in the iron-based superconductor $Ba_{0.6}K_{0.4}Fe_2As_2$ from scanning tunneling spectroscopy. *Phys. Rev. Lett.* **108**, 227002 (2012).

S9. Wang, Z., Yang, H., Fang, D., Shen, B., Wang, Q. H., Shan, L., Zhang, C., Dai, P. & Wen, H. H. Close relationship between superconductivity and the bosonic mode in $Ba_{0.6}K_{0.4}Fe_2As_2$ and $Na(Fe_{0.975}Co_{0.025})As$. *Nature Phys.* **9**, 42-48 (2013).

S10. Diallo, S. O. *et al.* Itinerant magnetic excitations in antiferromagnetic $CaFe_2As_2$. *Phys. Rev. Lett.* **102**, 187206 (2009).

S11. Mittal, R. *et al.* Measurement of anomalous phonon dispersion of $CaFe_2As_2$ single crystals using inelastic neutron scattering. *Phys. Rev. Lett.* **102**, 217001 (2009).